



Nonreciprocal interactions give rise to fast cilium synchronization in finite systems

David J. Hickey^a, Ramin Golestanian^{a,b,1}, and Andrej Vilfan^{a,c,1}

Edited by Monica Olvera de la Cruz, Northwestern University, Evanston, IL; received May 1, 2023; accepted August 14, 2023

Motile cilia beat in an asymmetric fashion in order to propel the surrounding fluid. When many cilia are located on a surface, their beating can synchronize such that their phases form metachronal waves. Here, we computationally study a model where each cilium is represented as a spherical particle, moving along a tilted trajectory with a position-dependent active driving force and a position-dependent internal drag coefficient. The model thus takes into account all the essential broken symmetries of the ciliary beat. We show that taking into account the near-field hydrodynamic interactions, the effective coupling between cilia even over an entire beating cycle can become nonreciprocal: The phase of a cilium is more strongly affected by an adjacent cilium on one side than by a cilium at the same distance in the opposite direction. As a result, synchronization starts from a seed at the edge of a group of cilia and propagates rapidly across the system, leading to a synchronization time that scales proportionally to the linear dimension of the system. We show that a ciliary carpet is characterized by three different velocities: the velocity of fluid transport, the phase velocity of metachronal waves, and the group velocity of order propagation. Unlike in systems with reciprocal coupling, boundary effects are not detrimental for synchronization, but rather enable the formation of the initial seed.

cilia | low Reynolds number hydrodynamics | metachronal waves | nonreciprocal interactions

Motile cilia are hairlike organelles which can move under their own power in order to fulfill roles such as fluid pumping or mixing (1). They are nigh-ubiquitous in biological systems, being found on most eukaryotic cells (2) including in the nervous system (3), the respiratory system (4), and the olfactory system (5). This makes them central to many open questions in biology, such as the precise mechanism behind the emergence of left–right differentiation during embryonic development (6). While the fascinating fluid dynamical questions involved in the dynamics of cilia and their biological function have been already highlighted by the pioneers of twentieth-century fluid dynamics, such as Prandtl (7) and Taylor (8), the subject of the collective properties of hydrodynamically active organelles at low Reynolds number continues to be an active field of research, particularly as a key component of the field of active matter (9).

When many motile cilia are located on a surface at sufficient density, their beating can synchronize with a phase lag between neighboring cilia. The resulting phase waves are called metachronal waves. It has been shown that metachronal coordination can lead to a high energetic efficiency of swimming or fluid transport (10, 11), and that metachronal waves may reduce collisions between cilia, further raising pumping speed (12). Moreover, the coordination has been shown to be beneficial for the efficiency of the chemosensory function of motile cilia (13). Metachronal waves are found in many different organisms and systems. For example, *Paramecium* uses metachronally coordinated cilia to swim (14), as well as to feed (14). Indeed, *Paramecium*'s swimming efficiency is close to the maximum possible efficiency for an organism with cilia of that length (10). Metachronal waves are found in other systems, such as the multicellular colony *Volvox* (15) or cilia in the respiratory tract (4) where their pumping efficiency is important for moving mucus (16). Metachronal coordination also appears in animals (e.g., krill) at larger length scales with very different coordination mechanisms (17).

Metachronal waves can be classified according to the direction of the wave propagation, depending on how the phase velocity of the wave compares to the direction of fluid transport. When these two directions are parallel, the metachronal wave is said to be symplectic. If they are antiparallel, the wave is called antiplectic (18). Other wave directions are classified as dexioplectic or leoplectic.

The fact that a pair of hydrodynamically interacting cilia or flagella can synchronize their cycles, even when belonging to two separate organisms (19), suggests that hydrodynamic coupling alone can be sufficient to explain the emergence of metachronal

Significance

Motile cilia are hairlike organelles that, at sufficient density, can synchronize hydrodynamically with their neighbors to form a metachronal wave. We use a minimal model of a ciliary carpet that accounts for near-field hydrodynamic coupling between cilia and show that the interaction between cilia can be nonreciprocal. We propose to characterize the collective dynamics of an array of cilia by three different velocities and their directions: the direction of fluid transport, the direction of metachronal waves (phase velocity), and the direction of order propagation (group velocity). The latter determines the time scale of synchronization. Near-field nonreciprocal interactions can therefore give rise to rapid emergence of metachronal waves.

Author affiliations: ^aDepartment of Living Matter Physics, Max Planck Institute for Dynamics and Self-Organization, 37077 Göttingen, Germany; ^bRudolf Peierls Centre for Theoretical Physics, University of Oxford, Oxford OX1 3PU, United Kingdom; and ^cDepartment of Condensed Matter Physics, Jožef Stefan Institute, 1000 Ljubljana, Slovenia

Author contributions: R.G. and A.V. designed research; D.J.H. performed research; D.J.H. and A.V. analyzed data; and D.J.H., R.G., and A.V. wrote the paper.

The authors declare no competing interest.

This article is a PNAS Direct Submission.

Copyright © 2023 the Author(s). Published by PNAS. This open access article is distributed under Creative Commons Attribution License 4.0 (CC BY).

¹To whom correspondence may be addressed. Email: ramin.golestanian@ds.mpg.de or andrej.vilfan@ds.mpg.de.

This article contains supporting information online at <https://www.pnas.org/lookup/suppl/doi:10.1073/pnas.2307279120/-DCSupplemental>.

Published September 27, 2023.

waves. Nevertheless, some studies also point to the additional role of intracellular linkages (20–22). In fact, the metachronal waves in *Paramecium* can preserve synchrony across the wall of a micropipette that isolates them hydrodynamically (23).

A fundamental problem in understanding synchronization via hydrodynamic interactions is the reversible nature of the Stokesian hydrodynamics, i.e. the fact that the fluid flow exactly reverses its direction upon the reversal of actuating forces, whereas the tendency of a system to reach an ordered state is by definition irreversible (9). Theoretical models therefore have to take into account higher-order effects that break the respective symmetries. These can include a second degree of freedom per cilium (24–29), the asymmetric spatial arrangement of cilia (30), a trajectory or driving force with sufficiently broken symmetries (28, 31–37), or a nonlinear driving mechanism that, for instance, switches the direction of force when a switch point is reached (11, 38–41).

When discussing the role of symmetries for ciliary synchronization, one has to keep in mind that reciprocity manifests itself differently for conservative or dissipative interactions. For conservative forces, Newton’s third law states that opposite forces are exerted on both interacting bodies. For hydrodynamic interactions, which are dissipative in their nature, the Lorentz reciprocal theorem (42) implies that the force on one body, caused by the motion of a second one with a given velocity, is identical to the force on the second body when the first body moves with the same velocity. Hydrodynamic interactions therefore act on both bodies with the same sign. The interplay of both interaction types is one possibility to facilitate ciliary synchronization (26). In active systems, nonreciprocal interactions can arise where the effect of the interaction on body A differs from that on body B, both in magnitude and direction (33, 43–49). For example, in the Vicsek model, particles or animals can be affected by other particles in front of them in a different way from those behind them. The orientation of hydrodynamically coupled rotors is a prime example of nonreciprocal coupling that leads to a rich phenomenology, including turbulent behavior via defect proliferation and annihilation (31).

A major open question is related to the scaling with the system size and the role of boundaries of the ciliated region. Recent theoretical work shows that the time needed to reach synchronization scales quadratically with the number of cilia (50). In principle, the metachronal wave vector of the final state is not uniquely determined. However, the basins of attraction of different solutions can greatly differ in size, leading to a strong preference for one state (50). Boundaries are often detrimental for synchronization because the cilia at the edge have a smaller number of nearest neighbors, which can affect their characteristic frequency, as demonstrated in a small 1D row of artificial oscillators (51). Boundary effects in a finite system can even lead to the emergence of a chimera state in which the oscillators split up into a coherent and an incoherent population (52). The vast majority of theoretical and computational studies focus on systems with periodic boundary conditions as a representation of generic, infinite systems (11, 26, 31, 32, 34, 38, 50, 53, 54). In nature, periodic circular 1D chains of cilia exist, for instance, the oral cilia of *Stentor* (55) or in starfish larvae (56). However, for topological reasons, 2D arrangements of cilia need open boundaries or topological defects, as it is impossible to have a polar field on the topology of a sphere without discontinuities.

In this paper, we show that the near-field effects (NFEs) between hydrodynamically coupled cilia can lead to an effective nonreciprocal interaction, where cilium A can affect the phase of cilium B more strongly than vice versa when averaged over

an entire ciliary beating cycle. As a result of this nonreciprocity, the metachronal order propagates through the array of cilia with a group velocity, which is not directly related to the velocity of the fluid transport or the phase velocity of metachronal waves. In a finite group of cilia, order then emerges at a boundary and propagates across the group in a time that scales linearly with the system dimension, an order of magnitude faster than an equivalent system without near-field hydrodynamics. We suggest that nonreciprocal coupling is key to understanding the fast emergence of synchronization in large ciliary carpets. The dynamics of the system are then characterized by three independent velocities: the velocity of fluid transport above the surface, the phase velocity of metachronal waves, and the group velocity with which the order propagates.

Results

Cilia are long and thin and beat with a time-irreversible whip-like stroke (1). Because of the complexity of the ciliary stroke, its description quickly leads to an intractable number of parameters. We therefore take a simplified approach common to many theoretical models (e.g., refs. 30, 34, and 35) and replace the cilium with a small sphere, pushed along a fixed trajectory by a position-dependent active force. The position of the sphere represents the tip position of a cilium and the active driving force represents the activity of dynein motors of the cilium’s axoneme. We thus consider a sphere of radius b moving on a fixed circular trajectory of radius a , with its center a distance h above a surface. The sphere is driven by an internal driving force $F^{\text{dr}}(\phi)$ and has an internal friction coefficient $\Gamma(\phi)$, both of which act in the tangential direction of the trajectory. The tilt of the trajectory is controlled by an angle χ such that when $\chi = \pi/2$, the trajectory lies in a plane parallel to the substrate beneath the cilium, shown in Fig. 1A.

This choice to model the cilia as single spheres on fixed tilted circular trajectories means that we neglect much of the fluid flow driven by the cilium closer to the surface, while preserving the irreversibility of the cilium beat—essential given the inherent irreversibility of synchronization. This approximation also replicates the pumping ability of the cilium: When the cilium is closer to the no-slip surface, it produces less fluid flow, and when it is

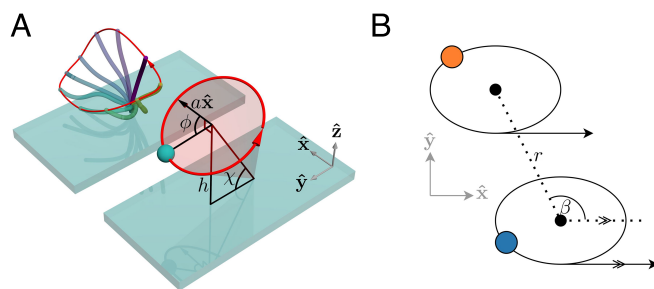


Fig. 1. Illustration of the model, showing the parameters used. (A) A realistic cilium motion with the trajectory shown in red. The power stroke (solid blue color) gives way to a slower recovery stroke along the no-slip surface of the substrate, resulting in net fluid flow in the direction of the power stroke over a cycle. Also shown is one of our model cilia that approximates the realistic motion, with the trajectory shown in red, and relevant quantities indicated. The circular trajectory retains the essential features of a power stroke far from the substrate and a recovery stroke much closer. (B) Definition of β and the intercilium distance r . The arrows represent the direction of the power stroke of the cilium, occurring at the highest point above the surface. Feathering on lines indicates that they are parallel, so that β is the angle between the power stroke and the displacement vector connecting the lattice points of two cilia.

further away it produces more. Over a cycle, the cilium moves a positive net amount of fluid in the direction of its “power stroke.” At distances from the cilium that are several times greater than h , this approximation gives almost identical fluid flow to a more detailed treatment of the cilium (57). In the following, we orient the pumping direction in the positive x -direction.

To study synchronization and the emergence of metachronal waves, we now consider many cilia arranged on a two-dimensional surface. Each point $\mathbf{r}_i = (x_i, y_i, 0)$ represents the position on the substrate directly below the center of a cilium’s trajectory. A pair of cilia (i and j) is characterized by the angle β_{ij} , which is the angle between the working stroke of cilium i (along the x -axis, Fig. 1) and the line pointing from \mathbf{r}_i to \mathbf{r}_j . These quantities are illustrated in Fig. 1B.

The position \mathbf{R}_i of the sphere representing cilium i is parameterized as a function of its phase ϕ_i following the notation used by Meng et al. (34):

$$\mathbf{R}_i(\phi_i) = \mathbf{r}_i + \begin{pmatrix} a \cos \phi_i \\ a \sin \phi_i \sin \chi \\ b - a \sin \phi_i \cos \chi \end{pmatrix}. \quad [1]$$

To replicate the beating cycle of a cilium, which consists of a fast working stroke followed by a slower sweeping recovery stroke, we introduce a position-dependent force and an internal drag coefficient, which together determine the force-velocity relationship of the active driving force $F^{\text{dr}}(\phi_i) - \Gamma(\phi_i)v$. Both can be expanded in a Fourier series as:

$$F^{\text{dr}}(\phi_i) = F_0^{\text{dr}} \left[1 + \sum_{n=1}^{\infty} A_n \cos(n\phi_i) + B_n \sin(n\phi_i) \right], \quad [2]$$

$$\Gamma(\phi_i) = \Gamma_0 \left[1 + \sum_{n=1}^{\infty} C_n \cos(n\phi_i) + D_n \sin(n\phi_i) \right]. \quad [3]$$

In the following, we only account for terms where $n \leq 2$. This simplification is justified, as the first harmonic is known to be essential for synchronization (and indeed is well-placed to replicate the cilium’s beating pattern of a fast power stroke and a slower recovery stroke), but the second harmonic is much more effective at driving the onset of synchronization and ensuring a more stable synchronized state (28, 35, 36).

Due to the linearity of the Stokes flow, the hydrodynamic force \mathbf{F}_i^{h} on a particle is a linear function of the particle’s own velocity and the velocities of all other particles it hydrodynamically interacts with. It can be expressed with a generalized friction tensor in the presence of a no-slip boundary, $\mathbf{\Gamma}(\phi_i, \phi_j)$, as $\mathbf{F}_i^{\text{h}} = -\sum_j \mathbf{\Gamma}(\phi_i, \phi_j) \cdot \mathbf{v}_j$. Along with the driving force, which is always tangential to the trajectory, and a perpendicular constraint force \mathbf{F}^{cstr} which keeps the particle on the trajectory, the force balance on cilium i states:

$$\mathbf{F}^{\text{dr}}(\phi_i) + \mathbf{F}^{\text{cstr}} - \mathbf{\Gamma}(\phi_i)\mathbf{v}_i - \sum_j \mathbf{\Gamma}(\phi_i, \phi_j) \cdot \mathbf{v}_j = 0. \quad [4]$$

By considering only its tangential component (i.e., multiplying the above equation with the tangent vector $\mathbf{t}(\phi_i)$), we obtain the equations of motion for each cilium:

$$F^{\text{dr}}(\phi_i) = \mathbf{\Gamma}(\phi_i)v_i + \sum_j \mathbf{t}(\phi_i) \cdot \mathbf{\Gamma}(\phi_i, \phi_j) \cdot \mathbf{t}(\phi_j)v_j. \quad [5]$$

Here, the velocities are related to the phase derivatives as $\mathbf{v}_i = (\partial \mathbf{R}_i / \partial \phi_i) \dot{\phi}_i$. By solving these equations numerically, we can

simulate the evolution of the cilium phases ϕ_i over time. In the following, we nondimensionalize all time units using the time period of an isolated cilium t_0 , which can be determined as $t_0 = \int_0^{2\pi} (\dot{\phi}_i)^{-1} d\phi_i$ using Eq. 5 without interacting neighbors.

Near Field Effects. We classify the near- and far-field effects based on a multipole expansion of the flow field around a beating cilium, which determines the interaction strength between two cilia. The relative strength of different multipole contributions is determined by the ratio between the intercilium distance r and the cilium height h .

The far-field hydrodynamics encompasses the effects in the leading order in r/h . The far field flow of a Stokeslet in the vicinity of no-slip boundary decays with the power $1/r^2$ radially, or $1/r^3$ along a direction parallel to the plane. Specifically, the far-field mobility tensor ($\mathbf{M} = \mathbf{\Gamma}^{-1}$) for two particles at a displacement $\Delta \mathbf{x} = (\Delta x, \Delta y, 0)$, where $\Delta x = x_j - x_i$ and $\Delta y = y_j - y_i$, takes the generic form (30)

$$\mathbf{M}(\mathbf{x}_i, \mathbf{x}_j) = \frac{3}{2\pi\eta} \cdot \frac{z_i z_j}{|\Delta \mathbf{x}|^5} \begin{pmatrix} (\Delta x)^2 & \Delta x \Delta y & 0 \\ \Delta y \Delta x & (\Delta y)^2 & 0 \\ 0 & 0 & 0 \end{pmatrix}. \quad [6]$$

Because the amplitude of a cilium’s motion (a) is of similar order as its height h , the variation of its horizontal position (x, y) also does not contribute to the leading term in the far-field expansion.

When the distance between cilia becomes closer, the next order in the multipole expansion needs to be taken into account. It consists of six independent terms that scale with $1/r^4$ and depends on the series expansion of the Green’s function, as well as on corrections due to the off-center positions of both cilia (57). We are referring to all interaction effects that become relevant when the intercilium distance is comparable to the height of the cilium (and therefore the trajectory radius) as NFEs. At even closer distances, the shape of the cilium becomes important and the approximation with a single sphere becomes inadequate.

Symmetries. Before discussing the numerical solutions, it is instructive to consider the symmetries of the system and their effect on synchronization and formation of metachronal waves. Our model contains the following symmetries:

1. Swapping. Because all cilia are intrinsically equal, the equations of motion stay the same when exchanging two cilia ($\phi_1 \leftrightarrow \phi_2$) and rearranging them such that $\beta \leftrightarrow \beta + \pi$.
2. Mirror symmetry. The trajectories of cilia (but not their drag and driving force) are symmetric with respect to $y \leftrightarrow -y$. The equations of motion therefore contain the symmetry $\beta \leftrightarrow \pi - \beta$, $\phi \leftrightarrow \pi - \phi$, $F_0^{\text{dr}} \leftrightarrow -F_0^{\text{dr}}$ with the adjustment of the coefficients defined in Eqs. 2 and 3: $(A_n, C_n) \leftrightarrow (-1)^n (A_n, C_n)$ and $(B_n, D_n) \leftrightarrow -(-1)^n (B_n, D_n)$.
3. Time reversal. Due to the time-reversibility of the Stokes equation, the equations of motion also remain invariant under the transformation $F_0^{\text{dr}} \leftrightarrow -F_0^{\text{dr}}$ and $t \rightarrow -t$. Because of the time reversal, a solution that is stable in the original system becomes unstable in the transformed system.
4. Without near-field hydrodynamics: axial reflection. If the distance between cilia is sufficient that the near-field hydrodynamic interactions can be neglected ($r \gg h$), the interaction term given by Eq. 6 becomes symmetric in space. The far-field mobility tensor is therefore symmetric with respect to $\beta \leftrightarrow \beta + \pi$.

The above symmetry properties have bold consequences for the synchronization. Consider a row of cilia arranged along the x axis, in the direction of pumping. In such a row, the angles β can only have values 0 and π . Without any of the coefficients that change sign under (ii), i.e., A_1, C_1, B_2, \dots , the motion is symmetric upon the combination of transformations (i), (ii), and (iii). Because the combined transformation contains time reversal which renders a stable solution unstable, no stable states are possible under these assumptions. The notion is consistent with the result in ref. 30 if two cilia are arranged along the pumping direction. The existence of a stable solution requires at least one of the terms $A_1, C_1, B_2, D_2, A_3, C_3$, etc., to be nonzero. The same argument also holds for a row of cilia arranged along the y axis (perpendicular to the pumping direction) when the symmetries (ii) and (iii) are employed (see related arguments in refs. 58 and 9).

Without NFEs in the hydrodynamic coupling, the symmetry property (iv) immediately implies the equivalence of metachronal waves with wave vectors \mathbf{k} and $-\mathbf{k}$, as seen in ref. 34. We therefore expect such systems to show the emergence of multiple long-lived domains with different metachronal wave vectors.

NFEs in combination with (for instance) the rotational motion of cilia can break the spatial symmetry, and lead to antisymmetric coupling terms that synchronize the cilia into a state with a nonzero phase difference (9, 30, 58–60). Here, we point out that the interactions are not only asymmetric with respect to the phase difference, but also nonreciprocal with respect to their strength. In a given configuration, the response of cilium i to the phase of cilium j can differ from the response of cilium j to cilium i both in the magnitude and in the phase dependence. This nonreciprocity has profound implications for the emergence of metachronal waves.

Synchronization in One Dimension. We first consider a one-dimensional row of cilia with uniform spacing d and open boundaries such that cilium i is located at position $\mathbf{r}_i = (id, 0, 0)$

(Fig. 2A). This means that $\beta_{ij} = 0$ or π for every cilium pair $i \neq j$. We used numerical simulations to see how order emerged in the system when the cilia were initialized with random initial phases.

Fig. 1B shows the phases of the cilia on a kymograph. The initially random phases quickly coalesce into mostly ordered waves, which slowly become more ordered over time until the waves are completely uniform. The average time t_s to reach a synchronized state scales approximately linearly with the system length (Fig. 1C). We consider the state as synchronized when the standard deviation (SD) of all cilium frequencies falls below a fixed threshold. The linear dependence can be understood by looking at the signal coherence between adjacent pairs of cilia (Fig. 1D). The signal coherence is a measure of the degree of linear dependence between two signals, given as a function of the frequency, with values between 0 and 1. For two signals in the time domain $x(t)$ and $x'(t)$, the coherence is calculated as:

$$C_{xx'}(f) = \frac{|\tilde{x}^*(f)\tilde{x}'(f)|^2}{\tilde{x}(f)\tilde{x}'(f)}, \quad [7]$$

where $\tilde{x}(f)$ and $\tilde{x}'(f)$ indicate the Fourier transforms of $x(t)$ and $x'(t)$, respectively. For every pair of cilia, we calculate the coherence between $\cos(\phi_i(t))$ and $\cos(\phi_j(t))$ at the frequency with the strongest cross-spectral density between the two signals (i.e., the frequency f that maximizes the numerator in Eq. 7).

Random patches of order sometimes emerge and travel against the pumping direction (in this case the pumping direction is rightwards), as the nonreciprocal nature of the hydrodynamic interactions causes the order to expand on one side and be extinguished by the disorder on its other side. However, when an ordered patch occurs close enough to the rightmost edge, there is no disorder to its right to extinguish it, so it spreads throughout the system. This explains why we see that the synchronization

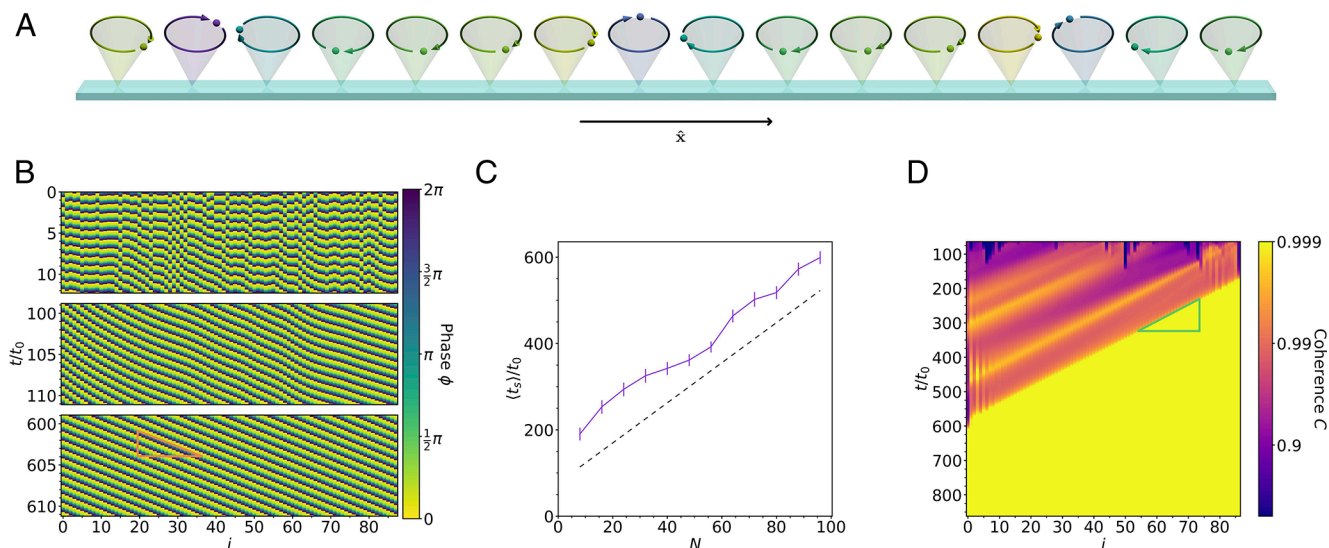


Fig. 2. Synchronization in a one-dimensional row of cilia. (A) A snapshot from the simulation. The colors indicate the phases. (B) A kymograph showing the metachronal waves in the system at different times. The simulation starts with random phases, but patches of order quickly assert themselves and give rise to waves that are initially uneven but eventually become completely uniform. The waves travel with the phase velocity v_{ph} (orange triangle) in the direction of fluid transport, and are hence symplectic waves. (C) The mean synchronization time (t_s) vs. the number of cilia N . The mean is calculated by simulating many systems at each size with different random initial phase configurations, and measuring how long it takes to synchronize using a metric based on SD of cilium frequencies. The figure shows that the synchronization time scales approximately linearly in the system size. Error bars are SEM, based on ≥ 92 simulations. (D) A kymograph showing the coherence between adjacent pairs of cilia. On this graph, each value of i on the abscissa corresponds to the coherence between cilium i and $i + 1$. Once an ordered patch forms on the right edge, it spreads across the row with the group velocity v_g (green triangle) in the negative x direction. The fact that the synchronization time is mainly limited by the propagation across the system explains the linear size-dependence in panel (C).

time has a roughly affine relationship with the system length.

Synchronization in Two Dimensions. The vast majority of motile cilia are found in two-dimensional bundles on multiciliated cells, where the cells themselves are sparsely distributed (61). Hence, we consider a two-dimensional square lattice with side length L and lattice constant d (so that the total number of cilia is $N = L \times L$). We enforce open boundaries and run a very similar simulation to the one described in the previous section. Fig. 3A shows the lattice, with the cilium trajectories marked according to their phase, rendering the structure of the metachronal wave clearly visible. Fig. 3B shows how the order of the cilia emerges over time: Initially, there is no correlation between phases, but over time some order emerges, which eventually solidifies into well-ordered metachronal waves.

Fig. 3C shows that the synchronization time scales approximately linearly with the linear dimension of the system L (i.e. $\langle t_s \rangle \sim L \sim \sqrt{N}$), just as in the one-dimensional case. This is

explained by Fig. 3D, which illustrates the coherence of each cilium with its neighbors. For each cilium i , the value is given by the geometric mean of coherence values with all directly adjacent (not including diagonally adjacent) cilia:

$$C_i^{\text{gm}} = \left[\prod_{j \in \{\text{n.n.}\}} C(\{\phi_i\}, \{\phi_j\}) \right]^{(1/N_{\text{n.n.}})}, \quad [8]$$

where $C(\{\phi\}, \{\phi'\})$ is the coherence, defined over two time series of phases. The resulting graph explains the linearity: The order emerges along one edge and gradually spreads across the entire lattice. Since the limiting factor to synchronization is the time taken for the order to spread through the length of the system, this time depends on the linear dimension as L/v_g .

The flow field induced by a carpet of cilia that has reached the synchronized state with steady metachronal waves is shown in Fig. 4. The time-averaged flows show a region of largely homogeneous flow above the carpet where the fluid is pumped

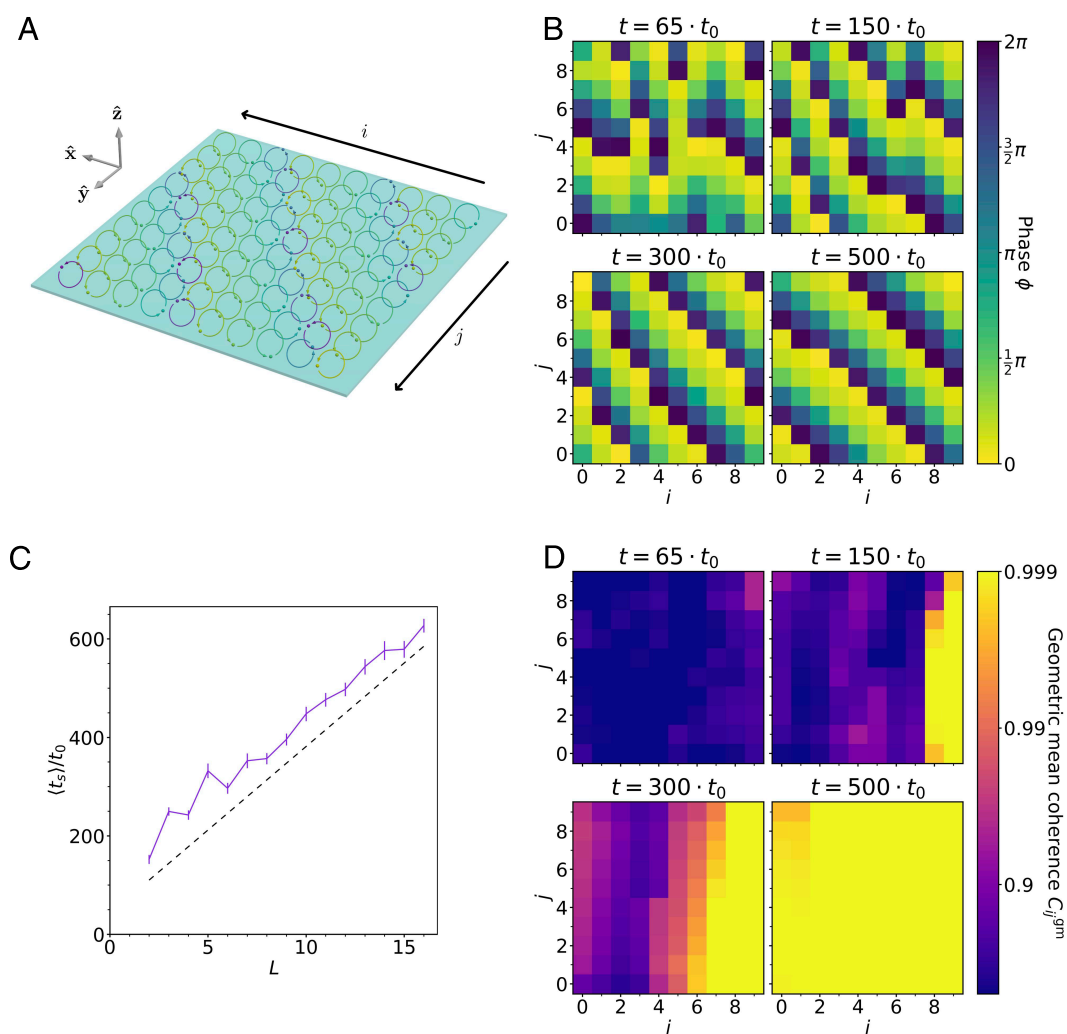


Fig. 3. Synchronization in a two-dimensional square lattice. (A) A schematic of the simulation of the square $L \times L$ lattice at a synchronized state for the specific case $L = 10$. The color of each model cilium indicates its phase, making the order clearly visible. See also [Movie S1](#) for an animated representation. (B) A series of snapshots showing the phases of the cilia in the square lattice, for the specific case of $L = 10$ (see [Movie S2](#) for a complete time series). (C) The mean synchronization time (t_s) vs. the linear dimension of the system L . The mean is calculated by simulating many systems at each size with different random initial phase configurations, and measuring how long it takes for the SD of the cilium frequencies in each system to drop below a certain threshold value. The synchronization time scales approximately linearly in L . Error bars are SEM, based on ≥ 31 samples. (D) The geometric mean of the coherence between each cilium and all of its neighbors for a specific simulation with $L = 10$. The order emerges on the right side and spreads across the system in negative x direction, leading to the observed linear dependence between the synchronization time and the length L .

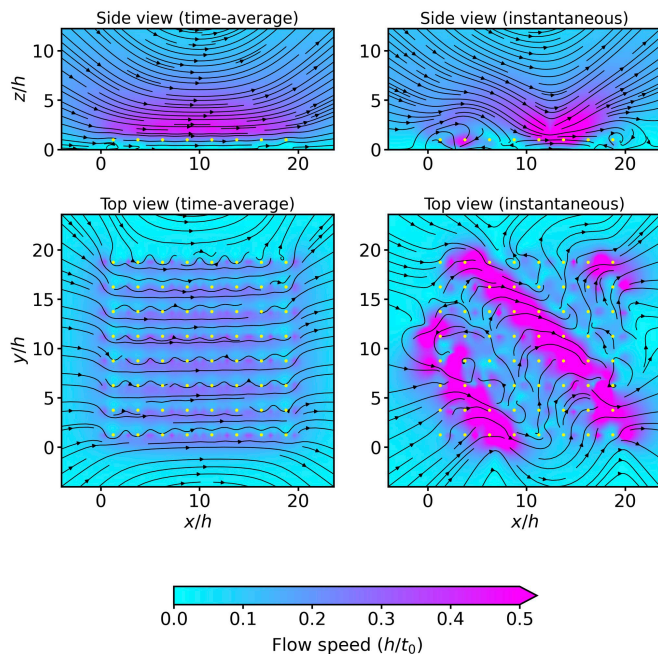


Fig. 4. Time-averaged and instantaneous flow in a system of 8×8 cilia after reaching a synchronized metachronal state. The background color indicates the flow speed in units of h/t_0 , and the yellow dots represent the center of cilium orbits. The side view corresponds to a vertical cross-section through the middle of the array of cilia ($x/h = 10$) and the top view to a slice at $z = h$. The structure of the metachronal wave is clearly visible in the instantaneous flow fields.

in the positive x -direction, the direction of the cilium power stroke. The instantaneous flows, on the other hand, show a periodic structure that follows the movement of metachronal wavefronts.

Although we used a square lattice as an example, the ability of cilia to synchronize is robust against the lattice type and the shape of the arrangement. Similar dynamics is obtained on a hexagonal lattice, as well as on an array with boundaries in the shape of an octagon (*SI Appendix, Fig. S1*).

Role of Nonreciprocity and NFEs. Our model shows strong nonreciprocity in the hydrodynamic interactions between cilia. This can be seen by calculating the effective coupling, which we define as the shift of beating frequencies caused by hydrodynamic interactions, relative to the unperturbed cilium ($\omega - \omega^{\text{unp}}$). The frequency shifts, averaged over one cycle, are shown in Fig. 5A as a function of the phase difference $\Delta\phi'$ and the relative position of the two cilia, represented by the angle β . Nonreciprocity manifests itself as shifts in the beating frequency of the two interacting cilia. The two cilia can experience dramatically different frequency shifts, with very different magnitudes and functional forms. The degree of this nonreciprocity is highly anisotropic, being much greater in the pumping direction than perpendicular to it (Fig. 5A). In a 1D row, the group velocity is approximately determined by the amplitude of the effective coupling in the direction in which it is stronger, as a function of phase (half the difference between its minimum and maximum). In the example shown, the amplitude is $10 \times 0.025/t_0$ (when rescaled to the coupling strength used elsewhere), suggesting $v_g \approx 0.25 d/t_0$. This agrees with the group velocity seen in Figs. 3 C and D and 5E.

As shown in *Symmetries*, nonreciprocal interactions are not possible when the hydrodynamic interactions are treated in the

far-field approximation. In the far-field, the interaction with a cilium at position β has to be identical to the interaction with a cilium at the opposite position $\beta + \pi$. We demonstrate this by disabling the NFEs and replacing the off-diagonal elements of the mobility matrix with the approximation given by Eq. 6. The resulting frequency shifts (dashed lines in Fig. 5A) become reciprocal, as they fulfill $\omega_1(\Delta\phi') = \omega_2(-\Delta\phi')$.

To investigate the role of NFEs in the formation of metachronal waves, we simulated the dynamics of a row of cilia (analogous to the results in Fig. 2) with only far-field interactions. The resulting synchronization times are significantly longer (orange line in Fig. 5B) than with NFEs (gray line). In small systems, the scaling with size becomes quadratic (inset in Fig. 5B), whereas we showed them to be linear in the presence of nonreciprocal coupling. However, in larger systems, the synchronization times saturate, as the final state no longer consists of a uniform metachronal wave. Rather, the system evolves into a long-lived state consisting of multiple domains with distinct wave vectors. An example with two domains, separated by one defect, is shown in Fig. 5D. The mean domain size and the likelihood that the system evolves into a monodomain metachronal wave are shown in Fig. 5C.

To understand the role of open boundaries in our system, we compared the results to the same system with periodic boundary conditions. Periodic boundary conditions are typical in other hydrodynamic models of ciliary or flagellar synchronization (11, 12, 26, 31, 32, 34, 38, 50, 53, 54, 62) when there are many cilia present [though with rare exceptions (e.g., ref. 41)], as they ensure that no cilia exist at an open boundary which could cause order to break down—indeed, when such models are subjected to open boundary conditions, they often find only intermittent synchronization (38). Our results show that introducing periodic boundaries, while preserving the nonreciprocal coupling, strongly increases the synchronization timescale, which again scales quadratically with the system size (Fig. 5B). The reason why periodic boundary conditions become deleterious to synchronization can be seen in the coherence kymograph in Fig. 5E. It shows a number of defects, each propagating with the group velocity v_g , that travel periodically across the system, so the system only slowly reaches a coherent state with a single metachronal wave.

Discussion

In our study, we used a strongly simplified model of a cilium. We replaced the cilium with a single particle moving along a tilted circular trajectory. The tilted trajectory breaks the most important symmetry of the cilium, namely that between the power stroke, when the distance to the surface is larger, and the recovery stroke, when the distance is smaller. This asymmetry is at the core of fluid transport, which does not rely on metachronal coordination, although the metachronal waves can improve the energetic efficiency of cilia (10, 11). At the same time, the driving force and the internal friction are modulated such that they reproduce a power stroke that is faster than the recovery stroke and also reproduce the fore-aft asymmetry that is present in cilia. The modulation of both parameters represents both the cyclic activity of dynein motors and the variations in the shape of the cilium, which is stretched during the power stroke and bent during the recovery stroke. Unlike theoretical models with fewer broken symmetries (35), our model allows the emergence of metachronal waves propagating with a group velocity that is not directly linked to the direction of fluid transport.

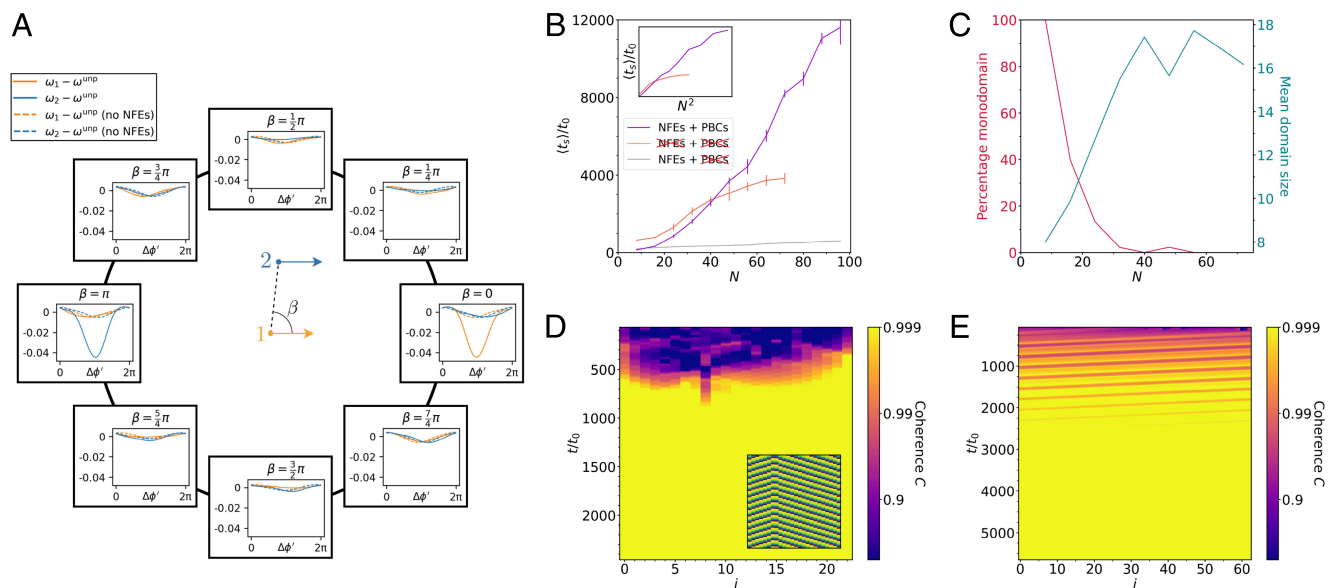


Fig. 5. The role of nonreciprocal hydrodynamic interactions and NFEs in synchronization. (A) The effective angular frequencies ω_1 and ω_2 of two interacting cilia (in dimensionless units) as a function of the adjusted difference $\Delta\phi'$. The cilia are positioned at a fixed distance ($r = 2.5h$) in different directions β . When the cilia are arranged in the x -direction ($\beta = 0, \pi$) there is a stark difference between ω_1 and ω_2 , showing that the interaction is highly nonreciprocal. The nonreciprocity is much weaker when the cilia are arranged in the y -direction ($\beta = \pi/2$), and the nonreciprocity vanishes entirely when near-field hydrodynamic effects are disabled (dashed lines). The interaction strength is reduced by a factor of 10 in order to stay in the linear regime. (B) The mean time to reach the synchronized state (t_s) in a 1D row of N cilia with NFEs disabled (orange) and with periodic boundary conditions (magenta). The synchronization time is dramatically longer in both of these cases than in the one-dimensional open boundary case (gray line, data from Fig. 2C). The inset indicates that the scaling of these synchronization times is close to $(t_s) \sim N^2$. With open boundaries and no NFEs, however, the synchronization time reaches a plateau when the final state consists of multiple domains with different wave vectors. Error bars are SEM based on nine samples for the periodic boundary case and ≥ 44 for the case without NFEs. (C) With NFEs disabled, the final state typically contains multiple domains with different wave vectors. The red line (left scale) shows the percentage of simulation runs that end in a monodomain state and the cyan line (right scale) the average domain size as a function of the system size N . (D) Kymograph showing the coherence between adjacent cilia with NFEs disabled, with the phase kymograph as an *Inset*. Unlike in the case of nonreciprocal coupling (Fig. 2D), defects between domains with different wave vectors remain after synchronization (the example shows one defect). (E) Coherence kymograph of the system with NFEs and periodic boundary conditions. Defects between coherent regions move with the group velocity but do not get extinguished at the boundaries, again resulting in a long synchronization time.

The numerical solution of the model equations takes into account not only the far-field hydrodynamics, as in ref. 34, but also the NFEs that become relevant when the size of a cilium becomes comparable to the distance between adjacent cilia. NFEs are definitely important in most ciliary systems that show metachronal coordination. For example, in *Paramecium* the intercilium distance is in the micrometer range, which is several times less than the cilium length (63). In respiratory epithelia, the distances are even shorter at fractions of a micrometer (64). On the other hand, in *Volvox* colonies, pairs of flagella (one on each cell) are spaced at a distance comparable to their length and still form metachronal waves (15). The intermediate densities we chose here allow us to take a generic approach that does not depend on fine details of the trajectory, while qualitatively capturing the near-field interactions. We therefore expect that the magnitude of NFEs, as well as interactions in general in our study, is underestimated and that the underlying principles can account for significantly faster synchronization in natural cilia.

Our main finding is that the NFEs can make the coupling nonreciprocal. The nonreciprocity goes beyond the asymmetry discussed in ref. 50, which implies that two cilia tend to synchronize with a phase difference that depends on their relative orientation. The nonreciprocal magnitude of the interaction means that a cilium tends to follow a neighbor on one side and to entrain the neighbor in the opposite direction. An easy-to-understand mechanism that contributes to nonreciprocity is that the periodically modulated driving force and internal drag make the cilium more susceptible to hydrodynamic interactions in certain parts of the trajectory, which are in turn closer to some

neighbors than others. The nonreciprocal coupling introduces a third direction in the plane, after the direction of fluid transport and the direction of the preferred metachronal wave, which dictates the propagation of order. We therefore refer to it as a group velocity. However, we note that unlike in classical waves in linear media with energy conservation, the group velocity is not related to the phase velocity in a straightforward way (e.g., through a dispersion relation). Although the near-field interactions and their effect on the coupling, even when restricted to the leading order, are more complex than far field, the nonreciprocity and the resulting order propagation are generic phenomena, which we expect to find across a wide range of model assumptions and parameter values.

Nonreciprocal coupling has two major effects on the formation of metachronal waves. First, it produces robust waves in finite systems with open boundaries. While open boundaries are the standard in real systems, they are detrimental in many models of synchronization, and also in experimental model systems (51). The majority of theoretical works on cilia synchronization therefore only investigate systems with periodic boundary conditions. In the presence of nonreciprocal coupling, the situation reverses and boundaries help seed the order which then rapidly spreads across the system. With nonreciprocal interactions, it is actually the periodic boundary conditions that significantly slow down the convergence to an ordered metachronal wave. The second major effect of nonreciprocal coupling is that the timescale of metachronal wave formation scales linearly with linear dimension of the system. This holds in both one and two dimensions, due to the linear spreading of order through the system from

a boundary. At each system size tested, as long as NFEs are not suppressed, the system always converges to the same metachronal wavevector regardless of the random initial conditions, meaning that the basin of attraction is effectively as large as the phase space of the system. We have demonstrated that suppressing the near-field hydrodynamic interactions (and therefore the nonreciprocal coupling) gives rise to unfavorable synchronization time scaling and unpredictable final states with long-living defects remaining.

Our model does not account for nonhydrodynamic interactions which have been shown to be relevant for cilium synchronization, such as steric effects (65) and basal coupling (22). Because it has been shown that hydrodynamic interactions alone are sufficient to achieve synchronization (66), one can consider these other effects as intercilium coupling to fine-tune the interactions rather than being an absolute requirement. In particular, basal coupling could provide a means to align metachronal waves in order to optimize efficiency (67). Finally, we neglected any inertial effects which are known to be small compared to viscous forces in systems of cilia. Nevertheless, it is still possible that a small inertial effect can be decisive for synchronization in situations where other effects cancel out (68, 69).

Our results leave some open questions that could be addressed in future work. For example, in real biological systems, there are a great many sources of noise (70), and at the scale of cilia, noise may be very relevant for synchronization (60) so future extensions to our model could examine the role of noise in the motion of the cilia. Additionally, we have assumed that all cilia are of identical lengths, but in reality, there can be variation in the lengths of cilia, and some studies have found that this can affect synchronization (71). Similarly, even in healthy humans, there are some cilia with structural abnormalities (72), which means that the influence on synchronization of nonidentical cilia may be significant. Our circular trajectory retains many key features of the stroke of real cilia, but it is possible that some crucial feature is lost in this simplification, so future work could integrate realistic cilium strokes with elongated cilia. This would also enable a more realistic driving engine for the cilia: In our model, the cilia have a time-varying driving force that always points along the tangent of the trajectory, but real cilia are driven by creating shear forces between pairs of dynein tubes that make up the internal structure of the cilium (73). It is possible that in the future, artificial or lab-grown cilia may have applications in microfluidic pumping, given the advancing state of the fields of growing artificial lab-on-a-chip cilia (74) and nanoscale artificial cilium production (75), which could offer real-world applications for our work and the future work proposed here.

Materials and Methods

Fluid Flow. At the scale of cilia, the behavior of the fluid flow field \mathbf{u} is well-approximated by the incompressible Stokes equations:

$$\begin{aligned} \eta \nabla^2 \mathbf{u} - \nabla p &= 0, \\ \nabla \cdot \mathbf{u} &= 0, \end{aligned}$$

where η is the fluid dynamic viscosity and p is the pressure.

The hydrodynamic interactions between two particles are calculated using a modified Rotne-Prager approximation with corrections to account for the no-slip fluid boundary on the surface below the cilium. The Rotne-Prager tensor takes into account terms up to the order $\sim r^{-3}$ and is equivalent to averaging Green's function (Oseen tensor) over the surfaces of both spheres. To take into

account the presence of the no-slip boundary at $z = 0$, we use the method of images and replace the free-space Green's function by the Blake tensor (76), defined as:

$$\begin{aligned} \mathbf{M}_{ij}^{\text{Blake}} &= \frac{1}{8\pi\eta} [\mathbf{G}^{\text{S}}(\mathbf{x}_i - \mathbf{x}_j) - \mathbf{G}^{\text{S}}(\mathbf{x}_i - \bar{\mathbf{x}}_j) \\ &\quad + 2z_j^2 \mathbf{G}^{\text{D}}(\mathbf{x}_i - \bar{\mathbf{x}}_j) - 2z_j \mathbf{G}^{\text{SD}}(\mathbf{x}_i - \bar{\mathbf{x}}_j)], \end{aligned} \quad [9]$$

where \mathbf{x}_k is the position of particle k , and $\bar{\mathbf{x}}_k$ is the position of the image of particle k reflected in the no-slip boundary at $z = 0$, and where:

$$\mathbf{G}_{\alpha\beta}^{\text{S}}(\mathbf{r}) = \frac{\delta_{\alpha\beta}}{r} + \frac{r_{\alpha} r_{\beta}}{r^3}, \quad [10]$$

$$\mathbf{G}_{\alpha\beta}^{\text{D}}(\mathbf{r}) = (1 - 2\delta_{\beta z}) \frac{\partial}{\partial r_{\beta}} \left(\frac{r_{\alpha}}{r^3} \right), \quad [11]$$

$$\mathbf{G}_{\alpha\beta}^{\text{SD}}(\mathbf{r}) = (1 - 2\delta_{\beta z}) \frac{\partial}{\partial r_{\beta}} \mathbf{G}_{\alpha z}^{\text{S}}(\mathbf{r}). \quad [12]$$

The Rotne-Prager tensor corrected for the no-slip boundary follows by including the leading corrections that result from surface-averaging over each sphere. The nondiagonal terms, describing the interaction between two particles $i \neq j$, can be calculated as:

$$\mathbf{M}_{ij} = \left(1 + \frac{a^2}{6} \nabla_{\mathbf{x}_i}^2 \right) \left(1 + \frac{a^2}{6} \nabla_{\mathbf{x}_j}^2 \right) \mathbf{M}_{ij}^{\text{Blake}}. \quad [13]$$

Explicit expressions for the elements of the mobility matrix can be found in ref. 77.

Solving Equations of Motion. The equations of motion as stated in Eq. 5 give a complete description of the system. However, they require the knowledge of the many-particle drag matrix $\mathbf{\Gamma}$, whereas the Rotne-Prager approximation gives us the mobility matrix $\mathbf{M} = \mathbf{\Gamma}^{-1}$. Simulating Eq. 5 directly for N cilia would therefore require the inversion of a $3N \times 3N$ matrix at each simulation step, in addition to solving a linear equation system with N unknowns.

To accelerate the numerical solution, we therefore rewrite the equations of motion based on the mobility matrix $\mathbf{M}(\phi_i, \phi_j)$ which gives the velocity response at the position of cilium i to a force at cilium j . We can express the force balance and the hydrodynamic equations with the hydrodynamic force \mathbf{F}_i^{h} acting on the cilium:

$$0 = \mathbf{t}_i \cdot \mathbf{F}_i^{\text{h}}(\{j\}) + F_i^{\text{dr}}(\phi_i) - \Gamma(\phi_i) v_i, \quad [14]$$

$$\mathbf{v}_i = -\mathbf{M}(\phi_i, \phi_i) \cdot \mathbf{F}_i^{\text{h}} - \sum_{j \neq i} \mathbf{M}(\phi_i, \phi_j) \cdot \mathbf{F}_j^{\text{h}}. \quad [15]$$

By multiplying the first equation with \mathbf{t}_i and inserting it into the second, we can derive a coupled set of $3N$ equations which allow us to solve for all hydrodynamic force vectors simultaneously (assuming that $\Gamma(\phi)$ is never zero):

$$\left(\mathbf{M}(\phi_i, \phi_i) + \frac{\mathbf{t}_i \mathbf{t}_i^{\text{T}}}{\Gamma(\phi_i)} \right) \cdot \mathbf{F}_i^{\text{h}} + \sum_{j \neq i} \mathbf{M}(\phi_i, \phi_j) \cdot \mathbf{F}_j^{\text{h}} = -\frac{F_i^{\text{dr}}(\phi_i)}{\Gamma(\phi_i)} \mathbf{t}_i.$$

In the above equation system, the first term describing the self-interaction of cilium i is always dominant, whereas the second term describing the hydrodynamic interactions between cilia is weaker and can be treated in a perturbative way. In matrix form, the equation is always block-diagonally dominant, which means that it can be solved efficiently using an adapted Successive Over-Relaxation (SOR) algorithm (78) that works on 3×3 blocks rather than individual elements. In the initial time step of the simulation, we use the solution to the purely diagonal matrix equation as the first iteration, but in subsequent steps, it is more efficient to start iterating with the solution of the previous step. In this way, only a very small number of iterations ($N_{\text{it}} = 3$) is required to converge to remarkably good accuracy with a relative error $\epsilon < 10^{-6}$. Once the hydrodynamic forces have been obtained, they can

be substituted back into Eq. 14 to find the cilium speeds v_j , and this can be trivially transformed into the time derivatives of the phases $\dot{\phi}_j$.

Numerical Integration. The phase of each cilium is updated using the standard Runge–Kutta method (RK4). Unlike implicit methods, Runge–Kutta algorithms require a single calculation of the hydrodynamic forces at each timestep, which is by far the most computationally demanding simulation step. The timestep used was approximately $0.001 t_0$.

Quantifying Synchronization. To determine whether the entire system has reached a synchronized state, we find the average frequencies of each cilium in a moving window of 50 time periods. We take the SD of these frequencies to be the order parameter of the system.

When considering pairs of cilia, as in Figs. 2C, 3D, and 5 D and E, SDs were less useful. Instead, the signal coherence was computed using the phases of adjacent pairs of cilia using Welch's method (79), with a moving window in the time domain representing approximately 50 unperturbed cilium cycles. In the 2D case, we instead used the geometric mean of the coherence with all neighboring cilia.

Uniform Phase Angle. In Fig. 5, we used a transformed phase difference $\Delta\phi' = \phi_2' - \phi_1'$. These angles have the property that for a single isolated cilium, ϕ' is constant. The transformed phase can be derived from the original phase angle using:

$$\phi'(\phi) = \frac{2\pi}{t_0} \int_0^\phi \frac{1}{\dot{\phi}(\phi'')} d\phi'', \quad [16]$$

where all quantities on the right-hand side are for an isolated cilium.

1. C. Brennen, H. Winet, Fluid mechanics of propulsion by cilia and flagella. *Annu. Rev. Fluid Mech.* **9**, 339–398 (1977).
2. M. V. Nachury, D. U. Mick, Establishing and regulating the composition of cilia for signal transduction. *Nat. Rev. Mol. Cell Biol.* **20**, 389–405 (2019).
3. R. Fabuel, C. Westendorf, E. Bodenschatz, G. Eichele, Cilia-based flow network in the brain ventricles. *Science* **353**, 176–178 (2016).
4. A. Yaghi, M. B. Dolovich, Airway epithelial cell cilia and obstructive lung disease. *Cells* **5**, 40 (2016).
5. V. Bhandawat, J. Reiser, K. W. Yau, Signaling by olfactory receptor neurons near threshold. *Proc. Natl. Acad. Sci. U.S.A.* **107**, 18682–18687 (2010).
6. A. Dasgupta, J. D. Amack, Cilia in vertebrate left–right patterning. *Philos. Trans. R. Soc. B: Biol. Sci.* **371**, 20150410 (2016).
7. L. Prandtl, Aufgaben der Strömungsforschung (Lecture delivered at the inauguration of the Kaiser Wilhelm Institute for Flow Research in Göttingen, 16 July 1925). *Naturwissenschaften* **14**, 335–338 (1926).
8. G. I. Taylor, Analysis of the swimming of microscopic organisms. *Proc. R. Soc. Lond. A* **209**, 447–461 (1951).
9. R. Golestanian, J. M. Yeomans, N. Uchida, Hydrodynamic synchronization at low Reynolds number. *Soft Matter* **7**, 3074 (2011).
10. N. Osterman, A. Vilfan, Finding the ciliary beating pattern with optimal efficiency. *Proc. Natl. Acad. Sci. U.S.A.* **108**, 15727–15732 (2011).
11. J. Elgeti, G. Gompper, Emergence of metachronal waves in cilia arrays. *Proc. Natl. Acad. Sci. U.S.A.* **110**, 4470–4475 (2013).
12. C. Ringers *et al.*, Novel analytical tools reveal that local synchronization of cilia coincides with tissue-scale metachronal waves in zebrafish multiciliated epithelia. *eLife* **12**, e77701 (2023).
13. D. Hickey, A. Vilfan, R. Golestanian, Ciliary chemosensitivity is enhanced by cilium geometry and motility. *eLife* **10**, e66322 (2021).
14. A. Funfak *et al.*, Paramecium swimming and ciliary beating patterns: A study on four RNA interference mutations. *Integr. Biol.* **7**, 90–100 (2015).
15. D. R. Brumley, M. Polin, T. J. Pedley, R. E. Goldstein, Hydrodynamic synchronization and metachronal waves on the surface of the colonial alga *Volvox carterii*. *Phys. Rev. Lett.* **109**, 268102 (2012).
16. S. Chateau, J. Favier, S. Poncet, U. D'Ortona, Why antiplectic metachronal cilia waves are optimal to transport bronchial mucus. *Phys. Rev. E* **100**, 791 (2019).
17. M. L. Byron *et al.*, Metachronal motion across scales: Current challenges and future directions. *Integr. Comp. Biol.* **61**, 1674–1688 (2021).
18. E. W. Knight-Jones, Relations between metachronism and the direction of ciliary beat in metazoa. *J. Cell Sci.* **3**, 503–521 (1954).
19. R. E. Goldstein, M. Polin, I. Tuval, Noise and synchronization in pairs of beating eukaryotic flagella. *Phys. Rev. Lett.* **103**, 168103 (2009).
20. K. Y. Wan, R. E. Goldstein, Coordinated beating of algal flagella is mediated by basal coupling. *Proc. Natl. Acad. Sci. U.S.A.* **113**, E2784–E2793 (2016).
21. G. Quaranta, M. E. Aubin-Tam, D. Tam, Hydrodynamics versus intracellular coupling in the synchronization of eukaryotic flagella. *Phys. Rev. Lett.* **115**, 238101 (2015).
22. Y. Liu, R. Claydon, M. Polin, D. R. Brumley, Transitions in synchronization states of model cilia through basal-connection coupling. *J. R. Soc. Interface* **15**, 20180450 (2018).

Periodic Boundary Conditions. When considering the effect of cilium j on cilium i , only the closest instance of j was considered. In simple terms, if j were right next to i , then we would proceed in the same way as if we had no periodic boundaries. However, if j were more than half of the system length away from i , then we would instead consider a copy of j translated by the system length, putting it closer to i . Since the mobility tensor decays quickly along the surface as $1/r^3$, neglecting the distant cilia does not have any effect on the results.

Numerical Parameters. In all simulations, we took the lattice constant to be $d = 2.5h = 2.5a$, and $b = a/10$. χ was always $\pi/6$ and we used $A_1 = -0.55$, $A_2 = -0.2$, $B_1 = -0.2$, $B_2 = 0.35$, $C_1 = 0.3$, $C_2 = -0.4$, $D_1 = -0.1$, and $D_2 = -0.55$. These parameters give a fast working stroke and a slower recovery stroke which break the fore–aft symmetry, consistent with the behavior of real cilia. The slowest part of the stroke is just before the lowest part of the recovery stroke, where the cilium would be curling up and the tip would therefore be traveling at its minimum speed. In Fig. 5A, the bead radius was reduced by a factor of 10 to $b = a/100$ in order to determine the linear order perturbation.

Data, Materials, and Software Availability. All study data are included in the article and/or supporting information.

ACKNOWLEDGMENTS. This work has received support from the Max Planck School Matter to Life and the MaxSynBio Consortium, which are jointly funded by the Federal Ministry of Education and Research (BMBF) of Germany, and the Max Planck Society. A.V. acknowledges support from the Slovenian Research Agency (grant no. P1-0099).

23. N. Naremsatsu, R. Quek, K. H. Chiam, Y. Iwamoto, Ciliary metachronal wave propagation on the compliant surface of *Paramecium* cells. *Cytoskeleton* **72**, 633–646 (2015).
24. M. Reichert, H. Stark, Synchronization of rotating helices by hydrodynamic interactions. *Eur. Phys. J. E* **17**, 493–500 (2005).
25. B. Guirao, J. F. Joanny, Spontaneous creation of macroscopic flow and metachronal waves in an array of cilia. *Biophys. J.* **92**, 1900–1917 (2007).
26. T. Niedermayer, B. Eckhardt, P. Lenz, Synchronization, phase locking, and metachronal wave formation in ciliary chains. *Chaos* **18**, 037128 (2008).
27. B. Qian, H. Jiang, D. A. Gagnon, K. S. Breuer, T. R. Powers, Minimal model for synchronization induced by hydrodynamic interactions. *Phys. Rev. E* **80**, 061919 (2009).
28. N. Uchida, R. Golestanian, Hydrodynamic synchronization between objects with cyclic rigid trajectories. *Eur. Phys. J. E* **35**, 135 (2012).
29. Y. Man, E. Kanso, Multisynchrony in active microfilaments. *Phys. Rev. Lett.* **125**, 148101 (2020).
30. A. Vilfan, F. Jülicher, Hydrodynamic flow patterns and synchronization of beating cilia. *Phys. Rev. Lett.* **96**, 1–4 (2006).
31. N. Uchida, R. Golestanian, Synchronization and collective dynamics in a carpet of microfluidic rotors. *Phys. Rev. Lett.* **104**, 178103 (2010).
32. N. Uchida, R. Golestanian, Synchronization in a carpet of hydrodynamically coupled rotors with random intrinsic frequency. *Europhys. Lett.* **89**, 50011 (2010).
33. S. Saha, S. Ramaswamy, R. Golestanian, Pairing, waltzing and scattering of chemotactic active colloids. *New J. Phys.* **21**, 063006 (2019).
34. F. Meng, R. R. Bennett, N. Uchida, R. Golestanian, Conditions for metachronal coordination in arrays of model cilia. *Proc. Natl. Acad. Sci. U.S.A.* **118** (2021).
35. A. V. Kanale, F. Ling, H. Guo, S. Fürthauer, E. Kanso, Spontaneous phase coordination and fluid pumping in model ciliary carpets. *Proc. Natl. Acad. Sci. U.S.A.* **119**, e2214413119 (2022).
36. N. Uchida, R. Golestanian, Generic conditions for hydrodynamic synchronization. *Phys. Rev. Lett.* **106**, 058104 (2011).
37. A. Maestro *et al.*, Control of synchronization in models of hydrodynamically coupled motile cilia. *Commun. Phys.* **1**, 1–8 (2018).
38. C. Wollin, H. Stark, Metachronal waves in a chain of rowers with hydrodynamic interactions. *Eur. Phys. J. E* **34**, 42 (2011).
39. H. Guo, L. Fauci, M. Shelley, E. Kanso, Bistability in the synchronization of actuated microfilaments. *J. Fluid Mech.* **836**, 304–323 (2018).
40. B. Chakrabarti, D. Saintillan, Hydrodynamic synchronization of spontaneously beating filaments. *Phys. Rev. Lett.* **123**, 208101 (2019).
41. B. Chakrabarti, S. Fürthauer, M. J. Shelley, A multiscale biophysical model gives quantized metachronal waves in a lattice of cilia. *Proc. Natl. Acad. Sci. U.S.A.* **119**, e2113539119 (2022).
42. H. Masoud, H. A. Stone, The reciprocal theorem in fluid dynamics and transport phenomena. *J. Fluid Mech.* **879**, P1 (2019).
43. R. Soto, R. Golestanian, Self-assembly of catalytically active colloidal molecules: Tailoring activity through surface chemistry. *Phys. Rev. Lett.* **112**, 068301 (2014).
44. R. Soto, R. Golestanian, Self-assembly of active colloidal molecules with dynamic function. *Phys. Rev. E* **91**, 052304 (2015).
45. J. Agudo-Canalejo, R. Golestanian, Active phase separation in mixtures of chemically interacting particles. *Phys. Rev. Lett.* **123**, 018101 (2019).

46. S. Saha, J. Agudo-Canalejo, R. Golestanian, Scalar active mixtures: The nonreciprocal Cahn-Hilliard model. *Phys. Rev. X* **10**, 041009 (2020).
47. S. A. M. Loos, S. H. L. Klapp, Irreversibility, heat and information flows induced by non-reciprocal interactions. *New J. Phys.* **22**, 123051 (2020).
48. M. Fruchart, R. Hanai, P. B. Littlewood, V. Vitelli, Non-reciprocal phase transitions. *Nature* **592**, 363–369 (2021).
49. S. Osat, R. Golestanian, Non-reciprocal multifarious self-organization. *Nat. Nanotechnol.* **18**, 79–85 (2023).
50. A. Solovev, B. M. Friedrich, Synchronization in cilia carpets: Multiple metachronal waves are stable, but one wave dominates. *New J. Phys.* **24**, 013015 (2022).
51. I. Kavre, A. Vilfan, D. Babič, Hydrodynamic synchronization of autonomously oscillating optically trapped particles. *Phys. Rev. E* **91**, 031002 (2015).
52. E. Hamilton, N. Bruot, P. Cicuti, The chimera state in colloidal phase oscillators with hydrodynamic interaction. *Chaos* **27**, 123108 (2017).
53. B. Nasouri, G. J. Elfring, Hydrodynamic interactions of cilia on a spherical body. *Phys. Rev. E* **93**, 033111 (2016).
54. F. O. Mannan, M. Jarvela, K. Leiderman, Minimal model of the hydrodynamical coupling of flagella on a spherical body with application to *Volvox*. *Phys. Rev. E* **102**, 033114 (2020).
55. K. Y. Wan *et al.*, Reorganization of complex ciliary flows around regenerating *Stentor coeruleus*. *Philos. Trans. R. Soc. B: Biol. Sci.* **375**, 20190167 (2020).
56. R. R. Strathmann, The feeding behavior of planktotrophic echinoderm larvae: Mechanisms, regulation, and rates of suspension-feeding. *J. Exp. Marine Biol. Ecol.* **6**, 109–160 (1971).
57. A. Vilfan, Generic flow profiles induced by a beating cilium. *Eur. Phys. J. E* **35**, 72 (2012).
58. G. J. Elfring, E. Lauga, Hydrodynamic phase locking of swimming microorganisms. *Phys. Rev. Lett.* **103**, 088101 (2009).
59. A. Solovev, B. M. Friedrich, Lagrangian mechanics of active systems. *Eur. Phys. J. E* **44**, 49 (2021).
60. A. Solovev, B. M. Friedrich, Synchronization in cilia carpets and the Kuramoto model with local coupling: Breakup of global synchronization in the presence of noise. *Chaos* **32**, 013124 (2022).
61. F. Boselli, J. Jullien, E. Lauga, R. E. Goldstein, Fluid mechanics of mosaic ciliated tissues. *Phys. Rev. Lett.* **127**, 198102 (2021).
62. A. Ghorbani, A. Najafi, Symplectic and antiplectic waves in an array of beating cilia attached to a closed body. *Phys. Rev. E* **95**, 052412 (2017).
63. K. Bouhouche *et al.*, *Paramecium*, a model to study ciliary beating and ciliogenesis: Insights from cutting-edge approaches. *Front. Cell Dev. Biol.* **10**, 847908 (2022).
64. M. A. Sleight, J. R. Blake, N. Liron, The propulsion of mucus by cilia. *Am. Rev. Respir. Dis.* **137**, 726–741 (1988).
65. R. Chelakkot, M. F. Hagan, A. Gopinath, Synchronized oscillations, traveling waves, and jammed clusters induced by steric interactions in active filament arrays. *Soft Matter* **17**, 1091–1104 (2021).
66. D. R. Brumley, K. Y. Wan, M. Polin, R. E. Goldstein, Flagellar synchronization through direct hydrodynamic interactions. *eLife* **3**, e02750 (2014).
67. A. W. J. Soh *et al.*, Intracellular connections between basal bodies promote the coordinated behavior of motile cilia. *Mol. Biol. Cell* **33**, br18 (2022).
68. M. Theers, R. G. Winkler, Synchronization of rigid microrotors by time-dependent hydrodynamic interactions. *Phys. Rev. E* **88**, 023012 (2013).
69. D. Wei, P. G. Dehnavi, M. E. Aubin-Tam, D. Tam, Measurements of the unsteady flow field around beating cilia. *J. Fluid Mech.* **915**, A70 (2021).
70. W. Gilpin, M. S. Bull, M. Prakash, The multiscale physics of cilia and flagella. *Nat. Rev. Phys.* **2**, 74–88 (2020).
71. M. Bottier, K. A. Thomas, S. K. Dutcher, P. V. Bayly, How does cilium length affect beating? *Biophys. J.* **116**, 1292–1304 (2019).
72. F. Verra *et al.*, Ciliary abnormalities in bronchial epithelium of smokers, ex-smokers, and nonsmokers. *Am. J. Respir. Crit. Care Med.* **151** (2013).
73. A. Horani, T. W. Ferkol, Advances in the genetics of primary ciliary dyskinesia. *Chest* **154**, 645–652 (2018).
74. J. C. Nawroth *et al.*, Stem cell-based lung-on-chips: The best of both worlds? *Adv. Drug Deliv. Rev.* **140**, 12–32 (2019).
75. J. M. J. den Toonder, P. R. Onck, Microfluidic manipulation with artificial/bioinspired cilia. *Trends Biotechnol.* **31**, 85–91 (2013).
76. J. R. Blake, A note on the image system for a stokeslet in a no-slip boundary. *Proc. Cambridge Philos. Soc.* **70**, 303–310 (1971).
77. M. Vilfan *et al.*, Self-assembled artificial cilia. *Proc. Natl. Acad. Sci. U.S.A.* **107**, 1844–1847 (2010).
78. D. M. Young, *Iterative Solution of Large Linear Systems* (Academic Press, Orlando, FL, 1971).
79. P. Welch, The use of fast Fourier transform for the estimation of power spectra: A method based on time averaging over short, modified periodograms. *IEEE Trans. Audio Electroacoust.* **15**, 70–73 (1967).